

Lattice Simulations with Effective Field Theory

Dean Lee^a, Evgeny Epelbaum^b, Hermann Krebs^b, Ulf-G. Meißner^{c,d}

^aDepartment of Physics, North Carolina State University, Raleigh, NC 27695, USA

^bInstitut für Theoretische Physik II, Ruhr-Universität Bochum, D-44870 Bochum, Germany

^cHelmholtz-Institut für Strahlen- und Kernphysik (Theorie) and Bethe Center for Theoretical Physics, Universität Bonn, D-53115 Bonn, Germany

^dInstitute for Kernphysik, Institute for Advanced Simulation, and Jülich Center for Hadron Physics, Forschungszentrum Jülich, D-52425 Jülich, Germany

E-mail: dean_lee@ncsu.edu

Abstract. Lattice effective field theory combines the theoretical framework of effective field theory with supercomputer lattice simulations. We discuss methods, recent results, and computational scaling for calculations of nuclei using lattice effective field theory. In particular we describe the calculation of the low-lying spectrum of carbon-12 and the scaling of computational resources needed for the calculation of other nuclei.

1. Introduction

Lattice effective field theory combines the theoretical framework of effective field theory with supercomputer lattice simulations. Effective field theory (EFT) is an organizational tool which reconstructs the interactions of particles as a systematic expansion in powers of soft scales such as particle momenta. Chiral EFT provides a systematic hierarchy of the forces among protons and neutrons. This approach comes with an estimate of the theoretical uncertainty at any given order in the chiral expansion which can be systematically reduced at higher orders. Over the past two decades, chiral EFT has proven a reliable and precise tool to describe the physics of few-nucleon systems. A recent review can be found in Ref. [1]. The low-energy expansion of EFT is organized in powers of Q , where Q denotes the typical momentum of particles. In chiral EFT the momentum scale Q is taken of the order of the mass of the pion times the speed of light. The most important contributions come at leading order (LO) or $O(Q^0)$. The next most important terms are at next-to-leading order (NLO) or $O(Q^2)$. The terms just beyond this are next-to-next-to-leading order (NNLO) or $O(Q^3)$. In the lattice calculations discussed here, we consider all possible interactions up to $O(Q^3)$. We also separate out explicitly the $O(Q^2)$ terms which arise from electromagnetic interactions (EM) and isospin symmetry breaking (IB) due to mass differences of the up and down quarks.

Several different *ab initio* approaches have been used to calculate the properties of few- and many-nucleon systems. This includes the no-core shell model [2, 3, 4, 5, 6], constrained-path [7, 8, 9, 10] and fixed-node [11, 12] Green's function Monte Carlo, auxiliary-field diffusion Monte Carlo [13, 14, 15], and coupled cluster methods [16, 17, 18]. Lattice effective field theory differs from other *ab initio* approaches in several respects. One difference is that many different phenomena can be studied in lattice EFT using the same lattice action. In principle

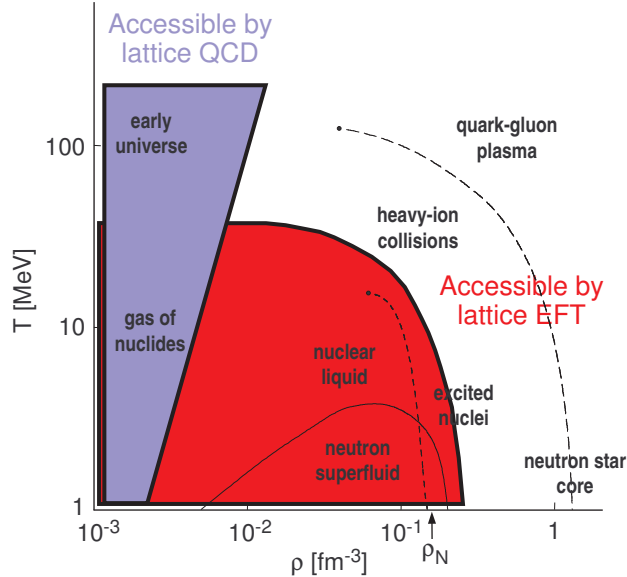


Figure 1. Phase diagram showing regions accessible by lattice QCD simulations and regions accessible by nuclear lattice EFT simulations.

all systematic errors are introduced up front when defining the low-energy effective theory, as opposed to the particular computational scheme used to calculate observables. Once the low-energy effective lattice action is determined, it may be used to calculate bound nuclei, transition matrix elements, the ground state of neutron matter, or bulk thermodynamic properties at nonzero temperature.

On the computational side lattice effective field theory is helped by efficient lattice methods developed for lattice QCD and condensed matter applications. This includes Markov Chain Monte Carlo techniques, auxiliary fields [19, 20], pseudofermion methods [21], and non-local updating schemes such as hybrid Monte Carlo [22, 23, 24]. Lattice effective field theory was first used in studies of infinite nuclear matter [25] and infinite neutron matter with pions [26] and without pions [27, 28, 29]. The method has also been used to study light nuclei in pionless effective field theory [30] and chiral effective field theory at leading order [31]. More recently dilute neutrons have been simulated at next-to-leading order in chiral effective field theory [32, 33] as well as light nuclei at next-to-next-to-leading order [34, 35]. As indicated in Fig. 1, lattice EFT is able to explore regions of the QCD phase diagram not accessible to lattice QCD. It also provides a test of duality between quark and hadronic descriptions in the region where the two methods overlap. Some recent developments in lattice effective field theory are reviewed in Ref. [36].

2. Methods

We simulate the interactions of nucleons using the Monte Carlo transfer matrix projection method introduced in Ref. [37]. Further details can be found in Ref. [31] as well as a recent review article [36]. Conceptually we are evolving the nucleons forward in Euclidean time while allowing them to interact as indicated in Fig. 2. In the actual lattice calculation, however, each nucleon evolves as if a single particle in a fluctuating background of pion fields and auxiliary fields. This is shown in Fig. 3. The interactions in Fig. 2 are reproduced after integrating over the fluctuating pion and auxiliary fields.

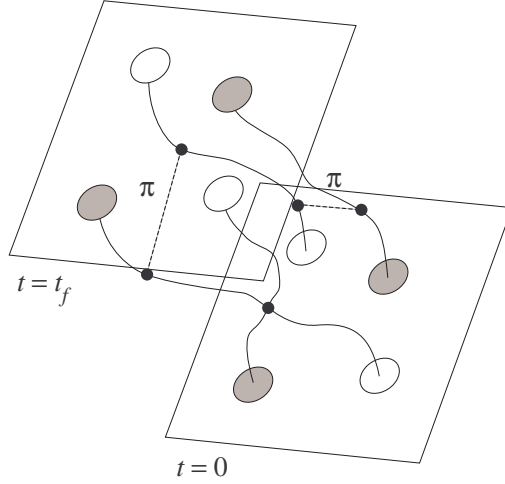


Figure 2. Worldlines of nucleons evolving in Euclidean time with contact interactions and the exchange of pions.

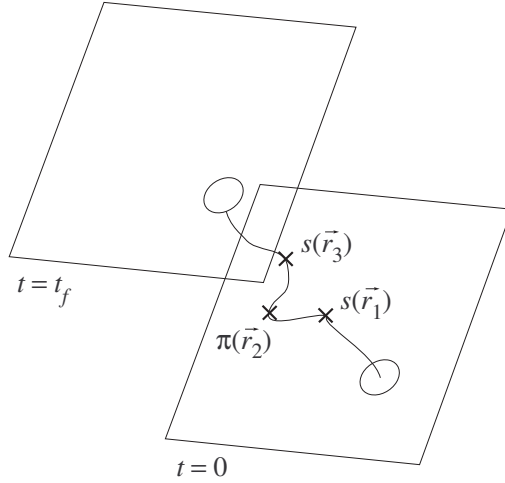


Figure 3. Worldline for a single nucleon evolving in a fluctuating background of pion fields and auxiliary fields.

The amplitude for a given configuration of pion and auxiliary fields is proportional to the determinant of an $A \times A$ matrix M_{ij} . The entries of M_{ij} are the single nucleon worldline amplitudes for a nucleon starting at momentum state j at $t = 0$ and ending at momentum state i at $t = t_f$.

Formally the leading-order calculation proceeds as follows. Let $|\Psi_{Z,N}^{\text{init}}\rangle$ be a Slater determinant of single-nucleon standing waves in a periodic cube for Z protons and N neutrons. Let H_{LO} denote the leading-order Hamiltonian including instantaneous one-pion exchange and contact interactions. Let $H_{\text{SU}(4)}$ be a Wigner $\text{SU}(4)$ -symmetric approximation to H_{LO} without pion exchange. Let us define a trial wavefunction

$$|\Psi(t')\rangle = \exp[-H_{\text{SU}(4)}t'] |\Psi_{Z,N}^{\text{init}}\rangle. \quad (1)$$

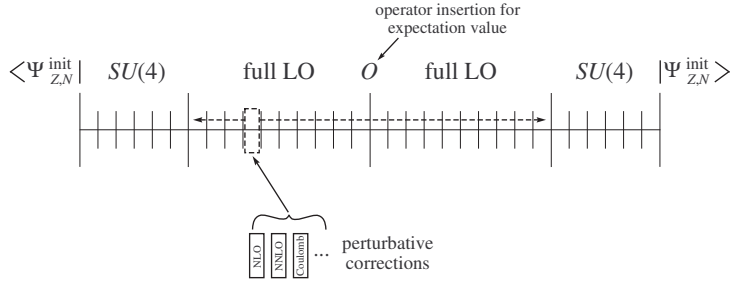


Figure 4. Schematic diagram of the transfer matrix calculation.

With this trial wavefunction we define the amplitude,

$$Z(t) = \langle \Psi(t') | \exp[-H_{\text{LO}}t] | \Psi(t') \rangle, \quad (2)$$

as well as an estimate of the energy,

$$E(t) = -\frac{\partial}{\partial t} [\ln Z(t)]. \quad (3)$$

In the limit of large t we get

$$\lim_{t \rightarrow \infty} E(t) = E_0, \quad (4)$$

where E_0 is the energy of the lowest eigenstate $|\Psi_0\rangle$ of H_{LO} with a nonzero inner product with $|\Psi(t')\rangle$. In order to compute the expectation value of some operator O we define

$$Z_O(t) = \langle \Psi(t') | \exp[-H_{\text{LO}}t/2] O \exp[-H_{\text{LO}}t/2] | \Psi(t') \rangle. \quad (5)$$

The expectation value of O for $|\Psi_0\rangle$ can be computed in the large t limit,

$$\lim_{t \rightarrow \infty} \frac{Z_O(t)}{Z(t)} = \langle \Psi_0 | O | \Psi_0 \rangle. \quad (6)$$

We use $\exp[-H_{\text{SU}(4)}t']$ as an approximate inexpensive low-energy filter and $\exp[-H_{\text{LO}}t]$ as an exact low-energy filter. The projection $\exp[-H_{\text{SU}(4)}t']$ is computationally inexpensive because the path integral for leading-order pionless effective field theory in the Wigner $SU(4)$ limit is strictly positive for any even number of nucleons [38]. Although there is no positivity theorem for odd numbers of nucleons, sign oscillations are also suppressed in odd systems when only one particle or one hole away from an even system with no sign oscillations. Higher order contributions, Coulomb repulsion, and isospin-breaking effects are computed as perturbative corrections to the leading-order transfer matrix. A schematic diagram of the transfer matrix calculation is shown in Fig. 4.

3. Recent results: Carbon-12 spectrum

Our collaboration has very recently completed *ab initio* lattice calculations of the low-energy spectrum of carbon-12 using effective field theory [39]. In addition to the ground state and excited spin-2 state, our calculations find a resonance at $-85(3)$ MeV with all of the properties of the Hoyle state and in agreement with the experimentally observed energy. The Hoyle state plays a crucial role in the hydrogen burning of stars heavier than our sun and in the production of carbon and other elements necessary for life. This excited state of the carbon-12 nucleus

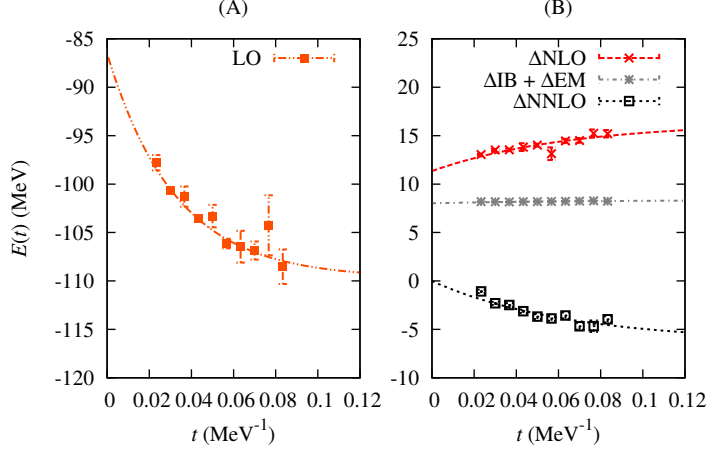


Figure 5. Lattice results for the ground state of carbon-12. Panel A shows the leading-order energy while Panel B shows corrections due to NLO, NLO with IB + EM, and NNLO interactions.

Table 1. Lattice results for the low-lying excited states of ^{12}C at LO, NLO, NLO with IB + EM, and NNLO. For comparison the experimentally observed energies are shown. All energies are in units of MeV.

	0_2^+	$2_1^+, J_z = 0$	$2_1^+, J_z = 2$
LO [$O(Q^0)$]	-94(2)	-92(2)	-89(2)
NLO [$O(Q^2)$]	-82(3)	-87(3)	-85(3)
IB + EM [$O(Q^2)$]	-74(3)	-80(3)	-78(3)
NNLO [$O(Q^3)$]	-85(3)	-88(3)	-90(4)
Experiment	-84.51	-87.72	

was postulated by Hoyle [40] as a necessary ingredient for the fusion of three alpha particles to produce carbon at stellar temperatures.

In Fig. 5 we show the ground state energy of carbon-12. Panel A plots the leading-order energy as a function of Euclidean time while Panel B shows higher-order corrections due to NLO interactions, NLO with isospin-breaking (IB) and electromagnetic (EM) interactions, and next-to-next-to-leading order (NNLO) interactions.

In Table 1 we show results for the low-lying excited states of ^{12}C at leading order (LO), next-to-leading order (NLO), next-to-leading order with isospin-breaking and electromagnetic corrections (IB + EM), and next-to-next-to-leading order (NNLO). All energies are in units of MeV. For comparison we list the experimentally observed energies. The error bars in Table 1 are one standard deviation estimates which include both Monte Carlo statistical errors and uncertainties due to extrapolation at large Euclidean time. Systematic errors due to omitted higher-order interactions can be estimated from the size of corrections from $O(Q^0)$ to $O(Q^2)$ and from $O(Q^2)$ to $O(Q^3)$.

In Fig. 6 we show lattice results used to extract the excited state energies at leading order. For each excited state we plot the logarithm of the ratio of the projection amplitudes, $Z(t)/Z_{0_1^+}(t)$, at leading order. $Z_{0_1^+}(t)$ is the ground state projection amplitude, and the slope of the logarithmic function at large t gives the energy difference between the ground state and the excited state. In Fig. 7 we present lattice results used to determine the higher-order corrections to the excited

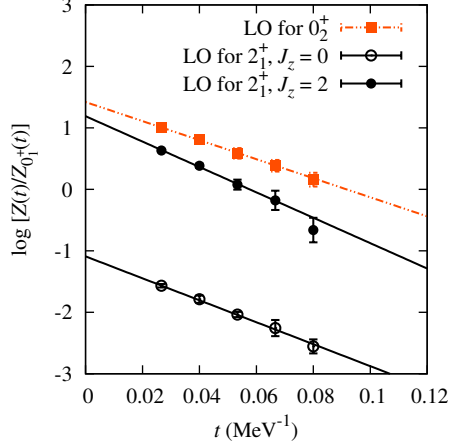


Figure 6. Extraction of the excited states of ^{12}C from the time dependence of the projection amplitude at LO. The slope of the logarithm of $Z(t)/Z_{0_1^+}(t)$ at large t determines the energy relative to the ground state.

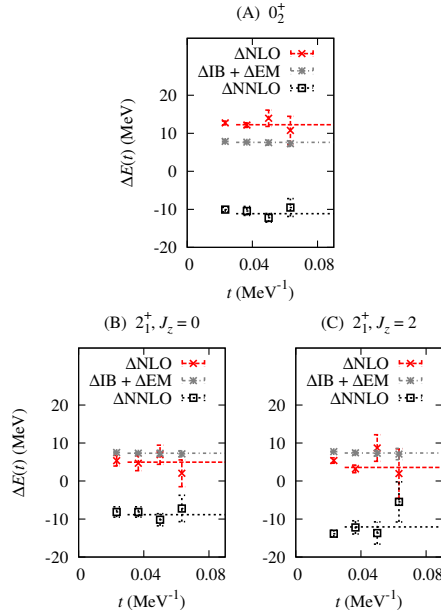


Figure 7. Higher-order corrections for the Hoyle state (A) and $J_z = 0$ (B) and $J_z = 2$ (C) projections of the spin-2 state. We show results versus projection time for corrections at NLO, NLO with IB + EM, and NNLO.

state energies. We show energies versus Euclidean time for corrections at NLO, NLO with IB + EM, and NNLO.

As seen in Table 1 and summarized in Fig. 8, the NNLO results for the Hoyle state and spin-2 state are in agreement with the experimental values. These results are the first *ab initio* calculations of the Hoyle state with an energy close to the phenomenologically important ^8Be -alpha threshold. Experimentally the ^8Be -alpha threshold is at -84.80 MeV, and the lattice determination at NNLO gives $-86(2)$ MeV. We also note the energy level crossing involving

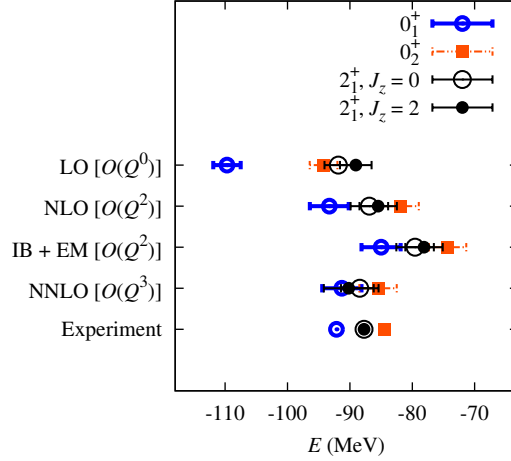


Figure 8. Summary of lattice results for the carbon-12 spectrum and comparison with the experimental values. For each order in chiral EFT labelled on the left, results are shown for the ground state (blue circles), Hoyle state (red squares), and the $J_z = 0$ (open black circles) and $J_z = 2$ (filled black circles) projections of the spin-2 state.

the Hoyle state and the spin-2 state. The Hoyle state is lower in energy at LO but higher at NLO. One of the main characteristics of the NLO interactions is to increase the repulsion between nucleons at short distances. This has the effect of decreasing the binding strength of the spinless states relative to higher-spin states. We note the 17 MeV reduction in the ground state binding energy and 12 MeV reduction for the Hoyle state while less than half as much binding correction for the spin-2 state. This degree of freedom in the energy spectrum suggests that at least some fine-tuning of parameters is needed to set the Hoyle state energy near the ^8Be -alpha threshold.

4. Computational scaling and performance

The very low memory and trivially parallel structure of the lattice Monte Carlo codes allow jobs to scale ideally with several thousand processors. In Fig. 9 we show the computational time for each processor on the BlueGene/P supercomputer JUGENE at the Jülich Supercomputing Center to generate one hybrid Monte Carlo (HMC) trajectory. The time is plotted as a function of the number of parallel processors. We see that the performance is entirely independent of the number of processors. The data shown is for a lattice simulation of carbon-12 in a periodic cube with length $L = 13.8$ fm.

Fig. 10 shows the computational time for a Xeon processor to generate one HMC trajectory versus the number of nucleons A . For this task the Xeon processor benchmarks at two and one-half times faster than a JUGENE processor. As the plot shows, the computational time scales as $A^{1.7}$ for these values of A . For smaller values the scaling is close to linear in A . The data shown is for lattice simulations of helium-4, beryllium-8, carbon-12, and oxygen-16 in a periodic cube with length $L = 13.8$ fm.

Fig. 11 shows the computational time for a Xeon processor to generate one HMC trajectory versus the lattice volume V . The computational time scales as $V^{1.5}$ for the volumes considered. The data shown is for lattice simulations of carbon-12 in periodic cubes with lengths $L = 9.9, 11.8, 13.8,$ and 15.8 fm.

Fig. 12 shows the average sign $\langle e^{i\theta} \rangle$ versus the number of nucleons A . The average sign

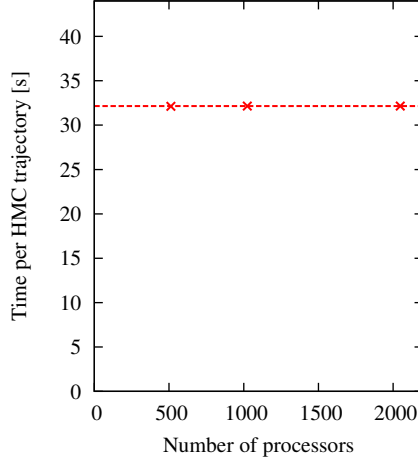


Figure 9. Computational time for each JUGENE processor to generate one HMC trajectory versus the number of parallel processors.

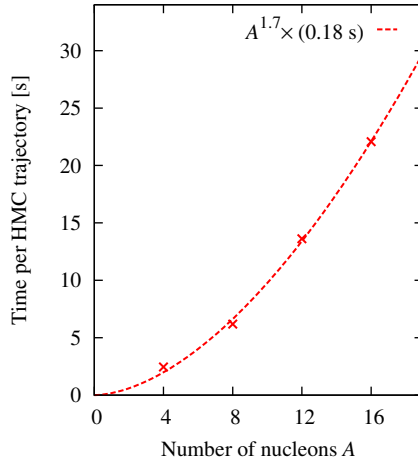


Figure 10. Computational time for a Xeon processor to generate one HMC trajectory versus number of nucleons A .

measures the severity of sign fluctuations in the Monte Carlo simulation of the lattice path integral. The average sign is approximately proportional to $e^{-0.11A}$. The data shown is for lattice simulations of helium-4, beryllium-8, carbon-12, and oxygen-16 in a periodic cube with length $L = 13.8$ fm.

5. Computational scaling for larger systems

Throughout this discussion we have kept the lattice spacing fixed. Decreasing the lattice spacing by a factor F will modify the required lattice volume by a factor of F^3 . That dependence is straightforward. However at this time there is no quantitative data on how much this affects the average sign. We base all estimates relative to simulations of the ground state of carbon-12 on a $L = 13.8$ fm periodic cube at lattice spacing $a = 1.97$ fm. This calculation in 2009 took about 12 rack-days on JUGENE. Algorithmic improvements in 2010 have reduced the same task to 2 rack-days on JUGENE. Each processor on JUGENE has a peak performance of 3.4 GFlop,

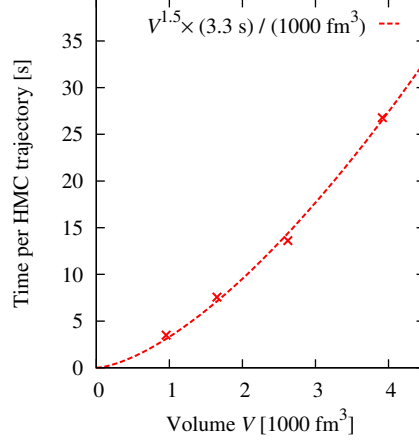


Figure 11. Computational time for a Xeon processor to generate one HMC trajectory versus lattice volume V .

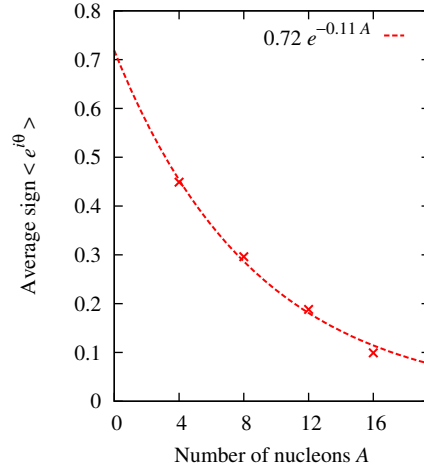


Figure 12. Average sign $\langle e^{i\theta} \rangle$ versus the number of nucleons A .

and each rack has 4096 processors. If we estimate the actual average performance of each processor to be 2 GFlops, the calculation requires about 4×10^{-5} PFlop-yr. Let us define

$$X_{12C}^{\text{CPU}} = 4 \times 10^{-5} \text{ PFlop-yr.} \quad (7)$$

In terms of RAM memory, the carbon-12 simulation uses $4A = 48$ nucleon degrees of freedom, 3 pion fields, and 16 auxiliary fields. The RAM memory required for the carbon-12 calculation is about 40 MB. We define

$$X_{12C}^{\text{RAM}} = 40 \text{ MB.} \quad (8)$$

With each simulation we store about 600,000 configurations, with each lattice configuration requiring about 3 MB of data. This comes to about 2 TB of archival disk storage. We define

$$X_{12C}^{\text{storage}} = 2 \text{ TB.} \quad (9)$$

At fixed volume and fixed number of configurations, the CPU scaling with nucleon number is about $A^{1.7}$. At fixed nucleon number and fixed number of configurations, the CPU scaling with

volume is about $V^{1.5}$. The average sign is more or less independent of volume, but with the 2010 version of the code it depends on the number of nucleons as $\exp[-0.11A]$. The number of required configurations for a given accuracy scales with the square of the reciprocal of the average sign. Since the average density of the nucleus is relatively constant, V scales linear with A . This gives the CPU scaling estimate

$$X^{\text{CPU}} \approx X_{12C}^{\text{CPU}} \times \left(\frac{A}{12}\right)^{3.2} \exp[0.22(A-12)]. \quad (10)$$

The RAM memory scales as

$$X^{\text{RAM}} \propto (4A + 16 + 3)V. \quad (11)$$

Since V is linear with A , we find

$$X^{\text{RAM}} \approx X_{12C}^{\text{RAM}} \times \left(\frac{A}{12}\right)^2. \quad (12)$$

The disk storage scales with the volume times the number of required configurations. Therefore

$$X^{\text{storage}} \approx X_{12C}^{\text{storage}} \times \left(\frac{A}{12}\right)^{1.5} \exp[0.22(A-12)]. \quad (13)$$

For nuclei with $S \neq 0$ or $I \neq 0$, the RAM memory formula in Eq. (12) still applies. The only computational difference is that the average sign will decrease. We estimate that the average sign will scale as

$$\exp[-1.5(S \bmod 2) - 2I], \quad (14)$$

where $S \bmod 2$ is the total spin S modulo 2 and I is the total isospin. This greatly oversimplifies the dependence, but probably is still a decent order-of-magnitude estimate in most cases.

This average sign modifies the CPU estimate,

$$X^{\text{CPU}} \approx X_{12C}^{\text{CPU}} \times \left(\frac{A}{12}\right)^{3.2} \exp[0.22(A-12) + 3(S \bmod 2) + 4I], \quad (15)$$

as well as the storage estimate,

$$X^{\text{storage}} \approx X_{12C}^{\text{storage}} \times \left(\frac{A}{12}\right)^{1.5} \exp[0.22(A-12) + 3(S \bmod 2) + 4I]. \quad (16)$$

Acknowledgements

Financial support acknowledged from the DFG (SFB/TR 16), Helmholtz Association (VH-VI-231), BMBF (grant 06BN9006), U.S. DOE (DE-FG02-03ER41260), EU HadronPhysics2 project ‘‘Study of strongly interacting matter’’, and ERC project 259218 NUCLEAREFT. Computational resources provided by the Jülich Supercomputing Centre at the Forschungszentrum Jülich.

References

- [1] E. Epelbaum, H.-W. Hammer, and U.-G. Meißner, Rev. Mod. Phys. **81**, 1773 (2009a), arXiv:0811.1338 [nucl-th].
- [2] C. Forssen, P. Navratil, W. E. Ormand, and E. Caurier, Phys. Rev. **C71**, 044312 (2005), nucl-th/0412049.
- [3] A. Nogga, P. Navratil, B. R. Barrett, and J. P. Vary, Phys. Rev. **C73**, 064002 (2006), nucl-th/0511082.
- [4] I. Stetcu, B. R. Barrett, and U. van Kolck, Phys. Lett. **B653**, 358 (2007), nucl-th/0609023.

- [5] P. Navratil, V. G. Gueorguiev, J. P. Vary, W. E. Ormand, and A. Nogga, Phys. Rev. Lett. **99**, 042501 (2007), nucl-th/0701038.
- [6] P. Maris, J. P. Vary, and A. M. Shirokov, Phys. Rev. **C79**, 014308 (2009), arXiv:0808.3420 [nucl-th].
- [7] S. C. Pieper, K. Varga, and R. B. Wiringa, Phys. Rev. **C66**, 044310 (2002), nucl-th/0206061.
- [8] S. C. Pieper, Nucl. Phys. **A751**, 516 (2005), nucl-th/0410115.
- [9] L. E. Marcucci, M. Pervin, S. C. Pieper, R. Schiavilla, and R. B. Wiringa (2008), arXiv:0810.0547 [nucl-th].
- [10] S. C. Pieper, B. Am. Phys. Soc. **54**, 70 (2009).
- [11] S. Y. Chang et al., Nucl. Phys. **A746**, 215 (2004), nucl-th/0401016.
- [12] A. Gezerlis and J. Carlson, Phys. Rev. **C77**, 032801 (2008), arXiv:0711.3006 [nucl-th].
- [13] S. Gandolfi, F. Pederiva, S. Fantoni, and K. E. Schmidt, Phys. Rev. Lett. **99**, 022507 (2007), arXiv:0704.1774 [nucl-th].
- [14] S. Gandolfi, A. Y. Illarionov, K. E. Schmidt, F. Pederiva, and S. Fantoni, Phys. Rev. **C79**, 054005 (2009a), arXiv:0903.2610 [nucl-th].
- [15] S. Gandolfi et al. (2009b), arXiv:0909.3487 [nucl-th].
- [16] M. Wloch et al., Phys. Rev. Lett. **94**, 212501 (2005), nucl-th/0501067.
- [17] G. Hagen, D. J. Dean, M. Hjorth-Jensen, T. Papenbrock, and A. Schwenk, Phys. Rev. **C76**, 044305 (2007), 0707.1516.
- [18] G. Hagen, T. Papenbrock, D. J. Dean, and M. Hjorth-Jensen, Phys. Rev. Lett. **101**, 092502 (2008), arXiv:0806.3478 [nucl-th].
- [19] J. Hubbard, Phys. Rev. Lett. **3**, 77 (1959).
- [20] R. L. Stratonovich, Soviet Phys. Doklady **2**, 416 (1958).
- [21] D. H. Weingarten and D. N. Petcher, Phys. Lett. **B99**, 333 (1981).
- [22] R. T. Scalettar, D. J. Scalapino, and R. L. Sugar, Phys. Rev. **B34**, 7911 (1986).
- [23] S. Gottlieb, W. Liu, D. Toussaint, R. L. Renken, and R. L. Sugar, Phys. Rev. **D35**, 2531 (1987).
- [24] S. Duane, A. D. Kennedy, B. J. Pendleton, and D. Roweth, Phys. Lett. **B195**, 216 (1987).
- [25] H. M. Müller, S. E. Koonin, R. Seki, and U. van Kolck, Phys. Rev. **C61**, 044320 (2000), nucl-th/9910038.
- [26] D. Lee, B. Borasoy, and T. Schäfer, Phys. Rev. **C70**, 014007 (2004), nucl-th/0402072.
- [27] D. Lee and T. Schäfer, Phys. Rev. **C72**, 024006 (2005), nucl-th/0412002.
- [28] D. Lee and T. Schäfer, Phys. Rev. **C73**, 015201 (2006a), nucl-th/0509017.
- [29] D. Lee and T. Schäfer, Phys. Rev. **C73**, 015202 (2006b), nucl-th/0509018.
- [30] B. Borasoy, H. Krebs, D. Lee, and U.-G. Meißner, Nucl. Phys. **A768**, 179 (2006), nucl-th/0510047.
- [31] B. Borasoy, E. Epelbaum, H. Krebs, D. Lee, and U.-G. Meißner, Eur. Phys. J. **A31**, 105 (2007), nucl-th/0611087.
- [32] B. Borasoy, E. Epelbaum, H. Krebs, D. Lee, and U.-G. Meißner, Eur. Phys. J. **A35**, 343 (2008a), arXiv:0712.2990 [nucl-th].
- [33] B. Borasoy, E. Epelbaum, H. Krebs, D. Lee, and U.-G. Meißner, Eur. Phys. J. **A35**, 357 (2008b), arXiv:0712.2993 [nucl-th].
- [34] E. Epelbaum, H. Krebs, D. Lee, and U. G. Meißner, Eur. Phys. J. **A41**, 125 (2009b), arXiv:0903.1666 [nucl-th].
- [35] E. Epelbaum, H. Krebs, D. Lee, and U.-G. Meißner, Phys. Rev. Lett. **104**, 142501 (2010), arXiv:0912.4195 [nucl-th].
- [36] D. Lee, Prog. Part. Nucl. Phys. **63**, 117 (2009), arXiv:0804.3501 [nucl-th].
- [37] D. Lee, Phys. Rev. **B73**, 115112 (2006), cond-mat/0511332.
- [38] J.-W. Chen, D. Lee, and T. Schäfer, Phys. Rev. Lett. **93**, 242302 (2004), nucl-th/0408043.
- [39] E. Epelbaum, H. Krebs, D. Lee, and U.-G. Meißner, Phys. Rev. Lett. **106**, 192501 (2011), 1101.2547.
- [40] F. Hoyle, Astrophys. J. Suppl. **1**, 121 (1954).